

# The Importance of Nanoscopic Ordering on the Kinetics of Photoinduced Charge Transfer in Aggregated $\pi$ -Conjugated Hydrogen-Bonded Donor–Acceptor Systems

Edwin H. A. Beckers,<sup>†</sup> Zhijian Chen,<sup>‡</sup> Stefan C. J. Meskers,<sup>†</sup> Pascal Jonkheijm,<sup>†</sup> Albertus P. H. J. Schenning,<sup>†</sup> Xue-Qing Li,<sup>‡</sup> Peter Osswald,<sup>‡</sup> Frank Würthner,<sup>\*,‡</sup> and René A. J. Janssen<sup>\*,†</sup>

Laboratory for Macromolecular and Organic Chemistry, Eindhoven University of Technology, PO Box 513, 5600 MB Eindhoven, The Netherlands, and Institut für Organische Chemie, Universität Würzburg, Am Hubland, D-97074 Würzburg, Germany

Received: April 21, 2006; In Final Form: July 1, 2006

Aggregated complexes of diaminotriazine oligo(*p*-phenylene vinylene) (OPV) units hydrogen bonded to different complementary perylene bisimide (PERY) compounds have been investigated by means of absorption, circular dichroism, photoluminescence, and photoinduced absorption spectroscopy. These studies reveal that in the aggregated state an ultrafast photoinduced charge separation occurs via an intermolecular pathway in the J-type stack of hydrogen-bonded OPV-PERY arrays. The subsequent charge recombination reaction strongly depends on small structural differences within the J-type geometry as revealed by comparison of stacked supramolecular dimers, trimers, and covalently OPV-PERY linked systems. A coupled oscillator model is used to analyze absorption and circular dichroism spectra and to identify intermolecular arrangements that are consistent with the experimental spectra and the charge-transfer kinetics.

## Introduction

The conversion of solar light in the photosynthetic reaction center<sup>1–4</sup> has inspired numerous studies on the photophysics of artificial donors–acceptor systems that exhibit a cascade of energy and electron-transfer reactions.<sup>5–12</sup> In addition to covalently linked systems, photoinduced energy and electron-transfer reactions in supramolecular assemblies based on hydrogen-bonding interactions also attracted considerable attention.<sup>13–36</sup> In contrast, the collective behavior of many chromophores as present in natural photosynthetic systems in photoinduced electron transfer has not received much attention in artificial systems.<sup>37</sup> Wasielewski et al. reported ordered photofunctional nanoparticles of tetrakis(peryene bisimide)-porphyrins in which the forward electron transfer is faster and the recombination slower compared to model compounds that do not form aggregates.<sup>38</sup> In other examples, photoinduced charge transfer has been up to an order of magnitude faster in thin films<sup>39</sup> or fine particles<sup>40</sup> as compared to the most polar solvents. In some examples charge separation rates exceeding  $10^{12} \text{ s}^{-1}$  have been observed in aggregated structures of donor–acceptor systems where the formation of a charge-separated state is not energetically favorable in the molecularly dissolved state.<sup>41–43</sup> We recently showed that in aggregates of covalently linked oligo(*p*-phenylene vinylene) (OPV)–peryene bisimide (PERY) triads (Ph-OPO, H-OPO, and Cl-OPO, Figure 1) the specific type of intermolecular packing can have tremendous consequences for the kinetics of the charge separation and recombination reactions.<sup>44</sup> For simple, vertically stacked aggregates (H-type) of donor–acceptor molecules the shortest distance between donor and acceptor is identical with the intramolecular distance and the rates for charge separation and

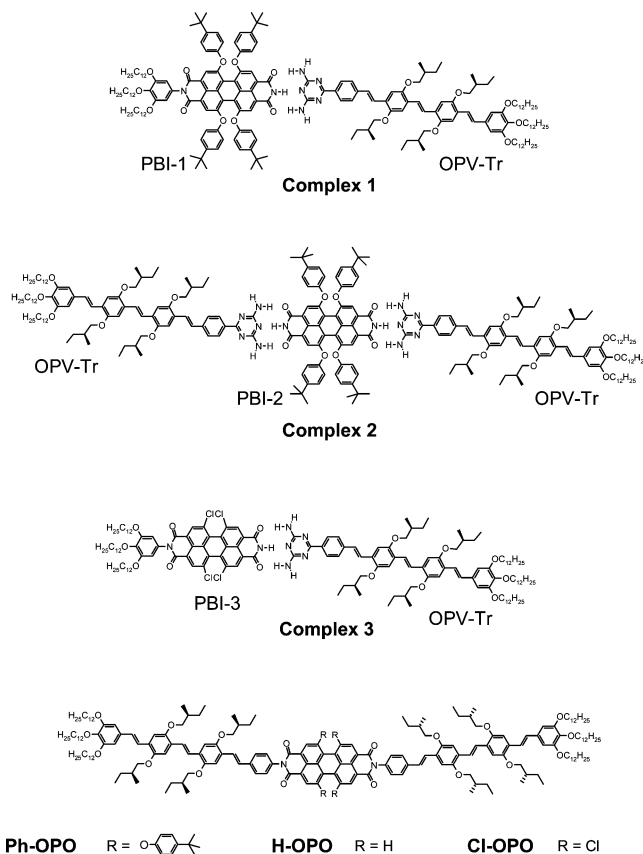


**Figure 1.** Structure of the diaminotriazine OPV-PERY complexes 1, 2, and 3 together with the covalent OPV-PERY-OPV triads Ph-OPO, H-OPO, and Cl-OPO.

recombination do not differ strongly in the aggregate form as compared to the molecule in solution (Figure 2). In contrast, for slipped, J-type packing configurations shorter intermolecular

\* Corresponding authors. E-mail: wuerthner@chemie.uni-wuerzburg.de and r.a.j.janssen@tue.nl.

<sup>†</sup> Eindhoven University of Technology.

<sup>‡</sup> Universität Würzburg.

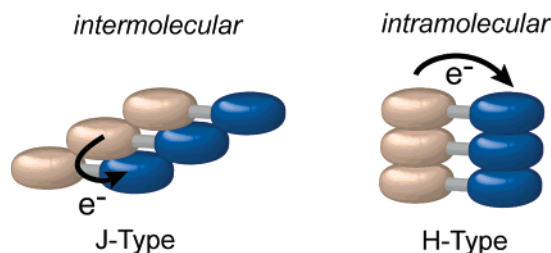


**Figure 2.** Cartoon of the two limiting situations for the one-dimensional packing of OPV-PERY arrays (OPV white, PERY blue) to give J-type (left) and H-type (right) aggregates and the shortest distance for electron transfer.

donor–acceptor distances arise in the assembly that increase the rates for forward and backward electron transfer. For the Ph-OPO, H-OPO, and Cl-OPO triads a more detailed investigation of the influence of intermolecular orientation on charge-transfer kinetics was hampered by the fact that in these covalent donor–acceptor–donor arrays the acceptor strength also changes. Furthermore we were interested to create systems where a very low driving force for intramolecular charge separation is expected to result in slow kinetics, while the intermolecular pathway in aggregates has a significantly enhanced rate for the same reaction.<sup>45</sup>

Herein we report a study of aggregate effects on the photoinduced electron-transfer reaction in hydrogen-bonded OPV-PERY complexes **1–3** (Figure 1) containing *tert*-butylphenoxy or chlorine substituents on the bay position of the PERY units. Previous work on complex **2**<sup>32,43</sup> has shown that the OPV and PERY chromophores in these complexes connect via a diaminotriazine–bisimide hydrogen bonding couple.<sup>46–50</sup> This unit has a “DAD” motif, complementary with the “ADA” motif of the imides of the PERY chromophore. A key advantage of this motif is that it is not self-complementary; hence formation of homodimers is less favored, leaving the OPV-PERY couples as the preferred hydrogen-bonded structure. As in Ph-OPO and Cl-OPO, the bay substituents in complexes **1–3** introduce torsion along the molecular axis that disfavors the vertical H-type packing of the molecules and results in a slipped, J-type packing.<sup>51</sup> This allows a comparison of the supramolecular arrays with their covalent analogues Ph-OPO and Cl-OPO and permits studying the effects of subtle differences in aggregation geometry within the J-type packing for arrays with the same (intramolecular) driving force for charge separation and recombination.

In the following we first describe the UV/vis absorption and circular dichroism (CD) spectra of complexes **1–3** in their molecularly dissolved and aggregated states. The spectra are subsequently analyzed in detail by using a coupled oscillator model to determine the intermolecular orientation of the OPV and PERY chromophores in the aggregated state. We demonstrate that J-type aggregation prevails for complexes **1–3**. Next, fluorescence and subpicosecond photoinduced absorption spectroscopy are used to reveal the excited-state behavior and determine rates for charge separation and recombination between OPV as donor and PERY as acceptor. We demonstrate that in the aggregated state an ultrafast photoinduced charge separation occurs via an intermolecular pathway in the J-type stack of hydrogen-bonded OPV-PERY arrays rather than intramolecular via the hydrogen-bonded pairs.

## Results and Discussion

**Synthesis and Electrochemistry of the Studied Compounds.** The synthetic routes to OPV-Tr,<sup>43</sup> PBI-2,<sup>46</sup> Ph-OPO,<sup>43</sup>

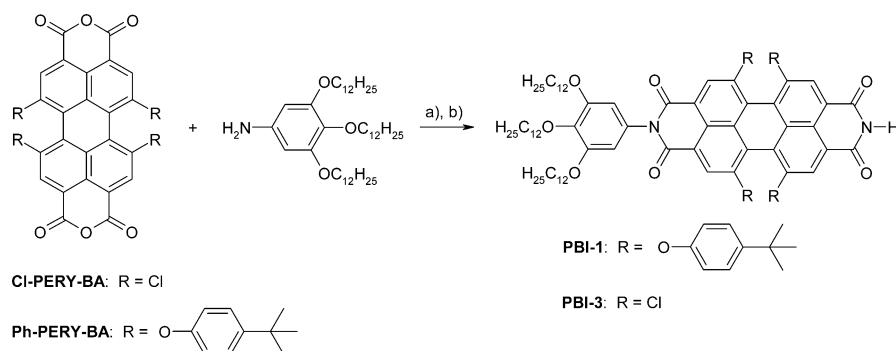
and Cl-OPO<sup>52</sup> (Figure 1) have been reported before. The two unsymmetrical perylene bisimides PBI-1 and PBI-3 were synthesized by monoimidization of the respective perylene bisanhydrides (Ph-PERY-BA and Cl-PERY-BA) with appropriate amounts of 3,4,5-tridodecyloxyaniline and subsequent reaction of the monoimide monoanhydrides with ammonium acetate (Scheme 1). The intermediate perylene monoimide monoanhydrides were used as crude products. The target perylene bisimide PBI-1 and PBI-3 were purified by silica gel chromatography and fully characterized by <sup>1</sup>H NMR, MS, and elemental analysis (see the Experimental Section for more details).

The oxidation and reduction potentials of the OPV-Tr and PBI-*n* have been determined by cyclic voltammetry in dichloromethane solution and the data are collected in Table 1.

**Phenoxy-Substituted OPV-PERY Systems.** Complex **1** comprises a perylene bisimide unit with four *tert*-butylphenoxy substituents at the bay positions and one trialkoxyphenyl at the imide position (PBI-1). This leaves only one side of the molecule available for complexation with the OPV-diaminotriazine (OPV-Tr) via hydrogen bonding. Evidence for aggregation of these complexes comes from concentration-dependent UV/vis absorption spectra recorded in methylcyclohexane (MCH). Clear spectral changes are observed upon increasing the concentration of complex **1** from  $2.6 \times 10^{-7}$  M to  $5.1 \times 10^{-4}$  M (Figure 3a). At low concentration, where molecularly dissolved species are expected, an absorption band with a maximum at 442 nm is observed that can be attributed to the OPV moiety. The band at 570 nm can be assigned to the lowest electronic transition of the PERY group and this band is accompanied by a vibronic replica at 530 nm. At higher concentrations both the OPV and the PERY absorption bands show a shift to longer wavelengths. This provides a strong indication for the presence of aggregated species of complex **1** and because of the red shift the aggregates may be classified as J-type. The molecular arrangement in the aggregates will be discussed in further detail below.

The temperature dependence of the aggregation of complex **1** in MCH has also been studied (Figure 3b). The absorption features recorded in MCH indicate that at a concentration of  $2 \times 10^{-4}$  M the molecules are aggregated at room temperature. Upon increasing the temperature, the absorption maximum shifts to the blue to a spectral position similar to that observed at low concentration at room temperature. This demonstrates that at higher temperatures the aggregates break up.

The observation of CD in the absorption of the aggregates provides evidence for a helical structure of the aggregates (Figure 3c). The loss of CD intensity at higher temperatures indicates dissolution of the aggregates. The CD spectrum at 5 °C shows a double bisignate (–/+–/+) couplet in the OPV and PERY absorption range. Bisignate Cotton effects are a characteristic of CD effects arising from interchromophoric interactions through exciton coupling between identical chromophores with a helical spatial arrangement. It should be noted that the individual components of complex **1**, when fully dissolved, give a negligible CD effect. The latter observation is consistent with the view that the stereocenters in both molecules are too far away from the  $\pi$ -system to induce an appreciable difference in the absorption of left and right circular polarized light. Upon aggregation, interchromophoric interactions come into play, and these can give rise to appreciable CD signals when the chromophores are arranged in a chiral way in space. We note that the intensity of the CD signal decreases more rapidly with increasing temperature than the shift of the absorption spectrum. This indicates that at elevated temperatures aggregates exist which have lost their helical internal structure

SCHEME 1: Synthesis of the Unsymmetrical Perylene Bisimide PBI-1 and PBI-3<sup>a</sup>

<sup>a</sup> Reagents and conditions: (a) zinc acetate, quinoline; Ar, 180 °C, 1.5 h; (b) ammonium acetate, propionic acid, reflux, 15 h.

**TABLE 1: Redox Potentials<sup>a</sup> of the Studied Compounds and the PERY(S<sub>1</sub>) Energy Levels Calculated from the Absorption Maximum in CH<sub>2</sub>Cl<sub>2</sub>**

compd	$E_{\text{ox}}(\text{OPV})$ (V)	$E_{\text{red}}(\text{PERY})$ (V)	PERY(S <sub>1</sub> ) (eV)
OPV-Tr	+0.33		
PBI-1		−1.17	2.12
PBI-2		−1.16	2.13
PBI-3		−0.81	2.38
Ph-OPO <sup>b</sup>	+0.34	−1.17	2.13
Cl-OPO <sup>b</sup>	+0.33	−0.80	2.38

<sup>a</sup> The redox potentials are referenced to the Fc/Fc<sup>+</sup> redox couple and were measured in CH<sub>2</sub>Cl<sub>2</sub> with 0.1 M NBu<sub>4</sub>PF<sub>6</sub> as supporting electrolyte. All compounds are molecularly dissolved at the used concentrations in CH<sub>2</sub>Cl<sub>2</sub>. <sup>b</sup> See ref 52.

due to thermal motion. For molecular aggregates it has also been predicted that the degree of circular polarization in absorption depends on the size of the aggregates,<sup>53–55</sup> and CD signals may be reduced because the average aggregate size is reduced by elevating the temperature.

Owing to the high solubility of tetraphenoxy-substituted perylene bisimides,<sup>56</sup> it is possible to create a supramolecular triad (complex **2**) consisting of two OPV-Tr units and one PERY moiety by using a symmetric perylene bisimide (PBI-2) instead of the asymmetric monoimide (PBI-1) as shown in Figure 1.<sup>32,43</sup> With the  $\pi$ -system significantly enlarged, it can be expected that aggregates of complex **2** are more stable than those created with the dimeric complex **1**. The absorption bands of the OPV and PERY moieties of complex **2** in MCH, when recorded at a concentration of  $5 \times 10^{-5}$  M and room temperature, are considerably red shifted in comparison with the corresponding absorption bands at high temperature or low concentration (Figure 4). This behavior indicates J-type aggregate formation in the case of low temperatures and relatively high concentration. The CD signal observed at low temperature supports a helical arrangement of the hydrogen-bonded complexes in the aggregates. The CD signal is lost at higher temperatures, consistent with the notion of aggregates breaking up.

**Chlorine-Substituted OPV-PERY Systems.** Complex **3** contains a perylene bisimide substituted with four chlorine atoms (PBI-3) instead of the phenoxy groups in PBI-1. Apart from this difference, its structure is the same as that of complex **1**. Concentration-dependent absorption spectra in MCH confirm aggregation behavior for this complex (Figure 5). Changes in the absorption spectrum are observed when increasing the concentration from  $2.0 \times 10^{-7}$  M to  $1.0 \times 10^{-5}$  M. The OPV moiety gives rise to an absorption band with a maximum at 442 nm. This band overlaps partially with the absorption spectrum of the Cl-substituted PERY. At 513 nm a shoulder in the absorption spectrum can be observed that is attributed to the 0–0 transition of the dissolved PBI-3 and the total spectrum

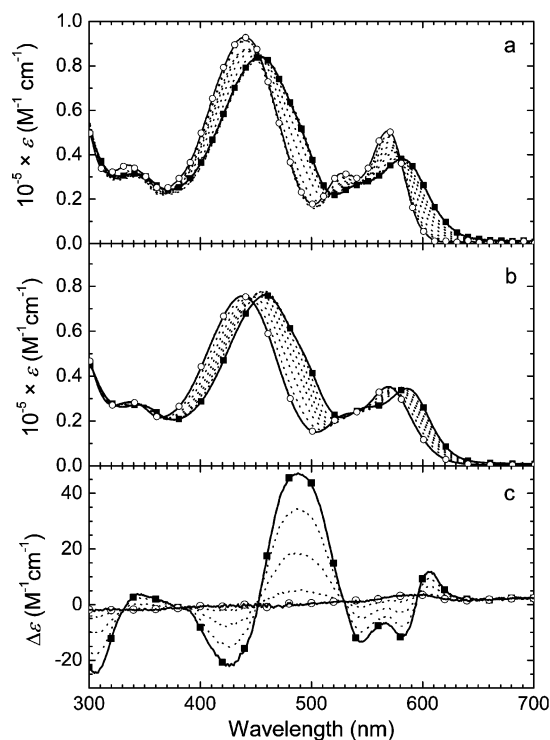


**Figure 3.** (a) Concentration-dependent UV/vis absorption spectra of complex **1** in MCH at room temperature. Concentrations range from  $2.6 \times 10^{-7}$  M (open circles) to  $5.1 \times 10^{-4}$  M (solid squares). (b) Temperature-dependent absorption spectra of complex **1** ( $2.0 \times 10^{-4}$  M in MCH) at temperatures from 20 °C (solid squares) to 90 °C (open circles). (c) Circular dichroism spectra of **1** ( $2.0 \times 10^{-4}$  M in MCH) between 5 (solid squares) and 25 °C (open circles).

is a superposition of the spectra of the individual compounds. At higher concentrations the absorption bands merge and the wavelength of maximal absorption shifts to 481 nm, indicating the presence of aggregated species of complex **3**. This red shift indicates a J-type structure at room temperature. The aggregation is further supported by the temperature dependence of the absorption spectra (Figure 5b) which points to dissolution of the aggregates at higher temperature. Also for the aggregates of complex **3** we observe a CD signal and, similar to the other complexes, the CD signal intensity reduces when raising the temperature. Although the CD gives strong evidence for a helically organized aggregated structure, it is difficult to explain the precise origin of the bisignate (−/+ ) CD signal because the absorption bands of the OPV and PERY chromophore overlap. The absorption and CD spectra for complex **3** may be compared to that for aggregates of Cl-OPO in MCH (see the Supporting Information, Figure S1). This compound shows a CD spectrum that is very similar to that of complex **3** but

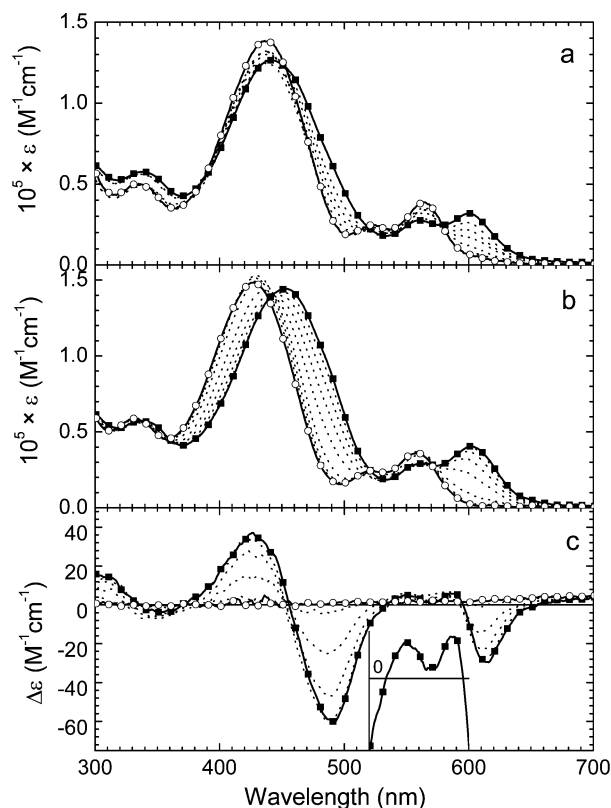


**Figure 4.** (a) Concentration-dependent UV/vis absorption spectra of complex 2 in MCH at room temperature. Concentrations range from  $1.0 \times 10^{-7}$  (open circles) to  $5.0 \times 10^{-5}$  M (closed squares). (b) Temperature-dependent absorption spectra of complex 2 ( $1.14 \times 10^{-5}$  M in MCH) between 10 (solid squares) and 90 °C (open circles) and (c) circular dichroism spectra of 2 ( $1.14 \times 10^{-5}$  M in MCH) recorded between 10 (solid squares) and 60 °C (open circles). The insert shows the 520–600 nm region of the CD spectrum (10 °C) on an expanded vertical scale.

opposite in sign even though the absolute chirality of the stereocenters on the side chains of the OPV is the same. This is consistent with the CD effect arising from interchromophoric couplings in aggregates whose internal structure is governed by weak intermolecular forces.

The stability of the three complexes can be analyzed in more detail by applying the isodesmic model to the results of the concentration-dependent absorption measurements (Figure 6).<sup>43</sup> According to this model complex 1 has an aggregation constant of  $8.3 \times 10^4 \text{ M}^{-1}$  ( $\Delta G^\circ = -28.0 \text{ kJ mol}^{-1}$ ), which is 1 order of magnitude smaller than the previously reported<sup>43</sup> value of  $1.5 \times 10^6 \text{ M}^{-1}$  ( $\Delta G^\circ = -35.2 \text{ kJ mol}^{-1}$ ) for the triad complex 2. An association constant of  $2.3 \times 10^6 \text{ M}^{-1}$  ( $\Delta G^\circ = -36.3 \text{ kJ mol}^{-1}$ ) is determined for complex 3. The significantly larger association constant for complex 3 as compared to complex 1 implies that the use of a chlorine-substituted perylene improves the stability of the aggregates in MCH, possibly as a result of an enhanced donor–acceptor interaction in the J-type packing, resulting from the fact that PBI-3 is a stronger acceptor than PBI-1 (Table 1). The association constant for complex 3 is also slightly higher than that observed for complex 2, indicating that the increased strength of the acceptor unit in complex 3 compensates for the smaller  $\pi$ -system with respect to complex 2.

**Simulation of the Absorption and CD Spectra and Analysis of Aggregate Packing.** Using a coupled oscillator model and approximating the interchromophoric interactions with the dipole–dipole interaction, we can simulate the absorp-

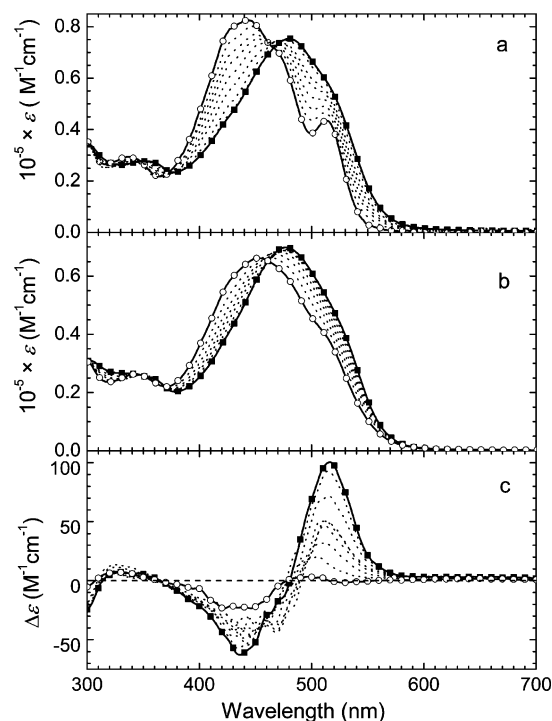


**Figure 5.** (a) Concentration-dependent UV/vis absorption spectra of complex 3 in MCH at room temperature in the range from  $2.0 \times 10^{-7}$  (open circles) to  $1.0 \times 10^{-5}$  M (solid squares). (b) Temperature-dependent absorption ( $1.0 \times 10^{-4}$  M, MCH) in the range 10 (solid squares) to 90 °C (open circles). (c) Circular dichroism spectra ( $1.0 \times 10^{-4}$  M, MCH) in the same temperature range.

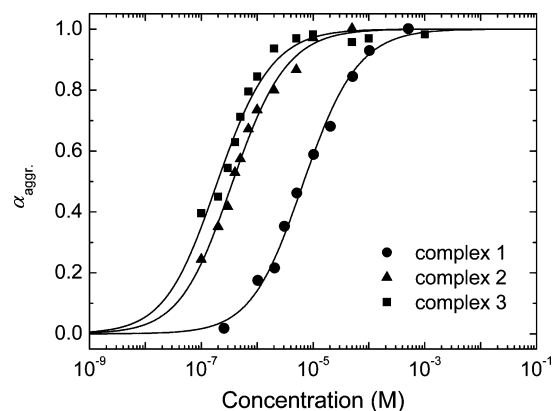


**Figure 6.** Fraction of aggregated component  $\alpha_{\text{agg}}$  as a function of the concentration of complex 1 (circles), complex 2 (triangles), and complex 3 (squares) in MCH at room temperature according to the isodesmic model.

tion and circular dichroism spectra of the aggregate assuming a particular mutual orientation of the chromophoric parts.<sup>57</sup> By calculating and simulating the absorption and CD spectra starting from various models for the structures of the aggregates and comparing the results with the experimental spectroscopic data discussed above, we will identify possible structures for the aggregates that are compatible with available spectroscopic data.

The simulation is semiempirical in nature and starts with extracting the magnitude of the transition dipole moments of the OPV and PERY chromophores from experimental data. The transition dipole moments for the transition from the ground state to the lowest excited singlet state for the isolated OPV and PERY moieties  $\vec{\mu}_{0,1}^Q$  ( $Q = A, B$ ;  $Q$  indicates a specific chromophore in the aggregate) are extracted from absorption spectra of the isolated compounds. For the mixed aggregates,



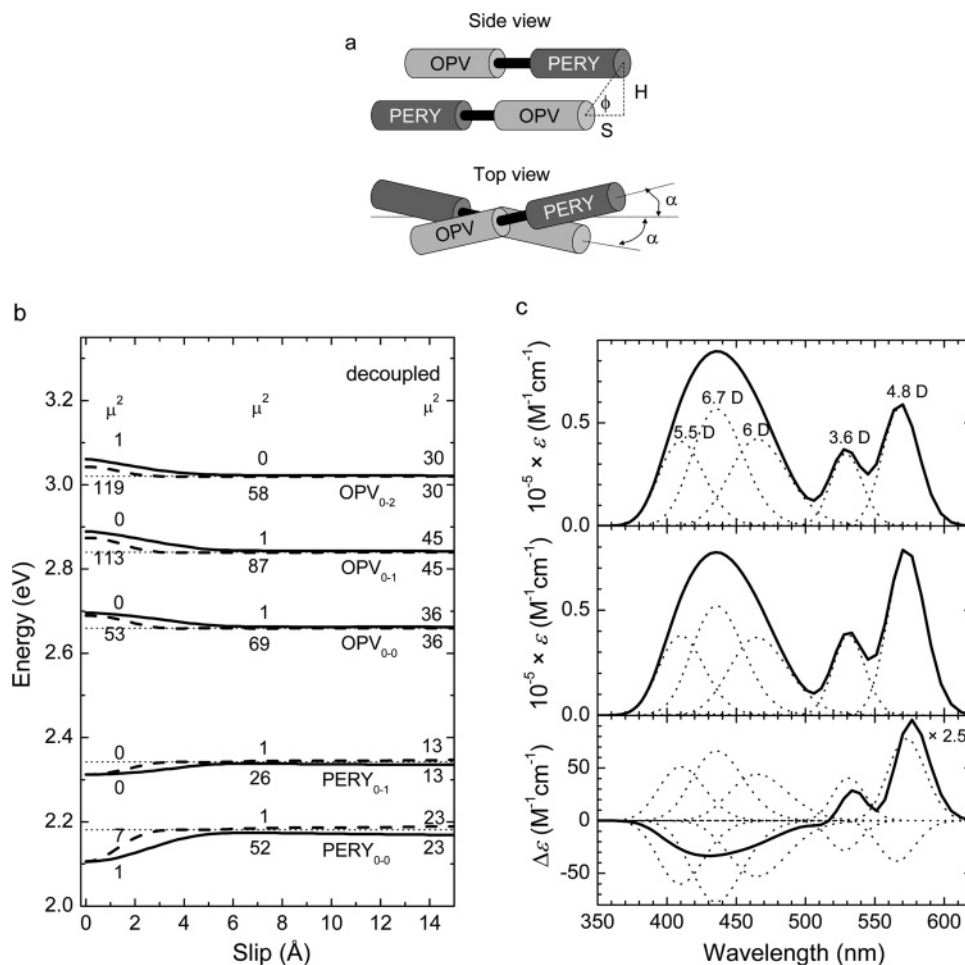


**Figure 7.** (a) Structural model for the aggregates of complex **1**. (b) Calculated excited-state energy levels as a function of the slip  $S$  ( $H = 5$  Å,  $\alpha = 5^\circ$ ). For  $S = 0$  and  $6$  Å, values for the square of transition dipole moment  $\mu$  (in Debye) are given for the transition between the excited and ground state. (c) Simulated spectra for  $S = 9$  Å. Upper panel: uncoupled chromophores. Dashed lines show the contribution from each vibronic transition. Transition dipole moments (in Debye) used in the calculation are given. Middle panel: simulated absorption spectra for the aggregated complex. Only one of the two vibronic Davydov levels carries appreciable intensity. Lower panel: simulated CD.

the pairwise interchromophoric interactions  $V$  are then calculated according to

$$V_{AB} = \frac{1}{4\pi\epsilon_0} \frac{[\vec{\mu}_{0,1}^A \cdot \vec{\mu}_{0,1}^B] \vec{R}_A - \vec{R}_B|^2 - 3[\vec{\mu}_{0,1}^A \cdot (\vec{R}_A - \vec{R}_B)][\vec{\mu}_{0,1}^B \cdot (\vec{R}_A - \vec{R}_B)]}{|\vec{R}_A - \vec{R}_B|^5} \quad (1)$$

where  $A$  and  $B$  denote either OPV or PERY chromophoric units and  $\vec{R}_A$  and  $\vec{R}_B$  are the position vectors for these chromophores. Excited-state energies and transition dipole moments can be obtained by diagonalizing the Hamilton matrix containing  $V_{AB}$  as off-diagonal matrix elements and the excited-state energies of the isolated chromophoric components on the diagonal (see the Supporting Information for more details). After diagonalization, the electrical and magnetic transition dipole moments  $\vec{\mu}_{0,i}$  and  $\vec{m}_{0,i}$  for the transition from the ground state to the collective states  $i$  are obtained for the coupled system

$$\vec{\mu}_{0,i} = \sum_{Q=1}^N c_{iQ} \vec{\mu}_{0,1}^Q \quad \text{and} \quad \vec{m}_{0,i} = i \sum_{Q=1}^N \alpha c_{iQ} (\vec{R}_Q \times \vec{\mu}_{0,1}^Q) \quad (2)$$

From these principal transition moments for the complex, the intensities of the absorption ( $\propto \vec{\mu}_{0,i} \cdot \vec{\mu}_{0,i}$ ) and circular dichroism bands [ $\propto \text{Im}(\vec{\mu}_{0,i} \cdot \vec{m}_{0,i})$ ] can be calculated. In this way the

experimental absorption and circular dichroism spectra can be compared with structural models.

The procedure followed is illustrated in Figure 7 for complex **1**. The absorption spectrum obtained at low concentration (Figure 3a) is simulated by taking a set of functions related to Gaussian curves with each curve representing a vibronic transition of either the OPV or the PERY chromophore. Vibronic fine structure is clearly visible in the absorption spectrum of the PERY chromophore (Figure 3) and two vibronic transitions (0–0 and 0–1) are included in the simulation. For the OPV chromophore, the vibronic fine structure is not visible at room temperature. Yet a number of low-temperature studies<sup>58–60</sup> have revealed a clear vibronic fine structure and the intense visible absorption band comprises three vibronic bands carrying appreciable intensity. The simulated spectrum is decomposed in the following way

$$\text{Abs}(\tilde{\nu}) = F_{\text{loc}} \sum_{j=1}^{10} \frac{|\vec{\mu}_j|^2 \tilde{\nu}}{C \sqrt{2\pi} \sigma_j} \exp \left[ -\frac{(\tilde{\nu} - \tilde{\nu}_j)^2}{2\sigma_j^2} \right] \quad (3)$$

Here,  $F_{\text{loc}}$  is the Lorentz local field correction,<sup>61</sup> which is related to the refractive index of the solvent.  $C$  is a constant (see the Supporting Information) and  $\mu_j$ ,  $\sigma_j$ , and  $\tilde{\nu}_j$  represent the transition dipole moment, the inhomogeneous bandwidth, and the center frequency of the vibronic transition  $j$ . The three panels

in Figure 7 illustrate the simulated absorption spectra for the decoupled chromophores (upper panel) and the aggregates (middle panel), and finally the circular dichroism for aggregates. For all three simulations we used the same set of values of  $\sigma_j$ , values which were optimized to reproduce the CD features. As a consequence, the peak intensities in the simulated absorption spectra of the isolated chromophores are not reproduced accurately. The values of  $\mu_j$  were determined in a separate simulation with  $\sigma_j$  values optimized for the absorption of the isolated chromophores.

The next step is the calculation of the collective excited states by diagonalization of the Hamiltonian describing the interchromophoric interactions. In this calculation we use the vibronic levels of the isolated chromophores as basis functions. This computational approach can be classified as the so-called weak coupling limit, where the interchromophoric couplings are assumed to be small in comparison with the energy gained by distortion of the nuclear geometry upon photoexcitation of the chromophore.<sup>53,62–64</sup> The advantage of this approach is its computational simplicity compared to a more accurate treatment that does not rely on separation of nuclear and electronic motion. However, the self-consistency of the weak coupling approach can be checked by comparing the predicted shifts in energy levels and the energy spacing between the vibronic levels.

A possible model structure for aggregates of complex **1** is illustrated in Figure 7. It represents a simple supramolecular aggregate in which two coupled OPV-PERY dimers are directly stacked on top of each other in an antiparallel fashion. The used model contains only two hydrogen-bonded complexes whereas the real aggregates may be much larger in size. The reduced aggregate size used in the modeling makes the calculations tractable. Furthermore, disorder in the real aggregates will limit the delocalization of the excited states and it may be expected that the essential spectroscopic features are determined on a very local scale, e.g., by the interactions between two neighboring hydrogen-bonded complexes. The results from the modeling should be interpreted in a qualitative way, as a guide for feasible structural elements in the aggregates.

In the structural model used, the slip  $S$ , which describes the sliding of the upper OPV-PERY hydrogen-bonded pair with respect to the underlying pair, is treated as an adjustable parameter. The height  $H$  is kept constant (5 Å) and the distance between the center of the OPV and PERY hydrogen bonded molecules is set at 20 Å. A helical arrangement of the chromophores is obtained by rotating the bottom OPV-PERY hydrogen bonded dimer over  $\alpha = -5^\circ$  and the upper dimer over  $+5^\circ$ .

The structural model can be used as input for calculating the interchromophoric couplings (eq 1). The excited-state energies calculated by solving the eigenvalue problem for the Hamiltonian matrix including the interchromophoric couplings are plotted in Figure 7 as a function of slip  $S$ . For small values of  $S$  the OPV and PERY based energy levels seem to “repel” with the PERY based energy levels shifting to lower energies. These changes can be understood in terms of the interchromophoric coupling between the OPV and PERY chromophores positioned right above each other. This coupling leads to a reduction of the dipole strength ( $\mu^2$ ) of the lower transitions and the intensity is shifted toward the higher lying OPV based levels. By increasing the slip, the lower transitions gain intensity and for  $S = 9$  Å we have simulated the full absorption and CD spectrum (Figure 7). After computation of the collective excited states, the simulated absorption spectrum can be constructed according to eq 3, using now the values for  $\mu_j$  and  $\tilde{\nu}0_j$  pertaining to the collective excited states. For the CD spectrum a similar procedure is followed (see the Supporting Information).

The structural model used as input supports the experimentally observed red shift of the PERY based transitions (at small  $S$ ) but fails to account for the red shift of the OPV based transitions and the circular dichroism spectrum. In the CD, the PERY based transitions show a positive Cotton effect while the OPV based transitions show a negative Cotton effect. This is indicative of relatively strong interchromophoric coupling between the OPV and PERY units and is not in agreement with the experimental spectra. Interestingly this type of CD spectrum has been observed experimentally for an OPV and PERY chromophore held in a cofacial chiral arrangement with the transition dipole moments pointing in almost the same direction.<sup>65</sup>

Better agreement between observed and simulated spectra can be obtained with the structural model illustrated in Figure 8a. Here, the two hydrogen-bonded OPV-PERY pairs are stacked in a parallel fashion. The distance between identical chromophores is now much smaller than the distance between the OPV and PERY units. Thus one may expect the interchromophoric interactions to be dominated by the PERY-PERY and OPV-OPV coupling. Indeed we find that degeneracy of the energy levels has lifted the levels and a Davydov splitting is observed for each vibronic level (Figure 8b). For small values of  $S$ , the high-energy Davydov level can be accessed from the ground state via an optically allowed transition while for larger values of  $S$  the transition to the lower Davydov level is allowed. The former behavior results in a blue shift of the absorption maximum (as observed for H-type aggregates) while the latter behavior can explain the spectroscopic features of J-type aggregates.<sup>66</sup> The switching point occurs when the angle between the transition dipole moments and the line joining the centers of the cofacial OPV and PERY chromophores is close to the magic angle ( $54^\circ$ ), which is around  $S = 3.5$  Å. The simulated absorption and CD spectra for  $S = 9$  Å, can reproduce a number of experimental observations: a red shift for both the OPV and PERY based absorption bands and their bisignate Cotton effects. The experimental CD spectrum (Figure 3) shows a double minimum in the 530–580 nm wavelength range that is reproduced, in a qualitative way, in the simulated spectra (Figure 8c). The decomposition of the simulated CD spectrum in the individual Gaussian bands shows that the two Davydov levels originating from the same vibronic energy level show CD effects opposite in sign. This may be expected in the case where the PERY-PERY and the OPV-OPV interchromophoric interactions dominate and the bisignate Cotton effect is commonly observed in chiral molecules containing two identical coupled chromophores. The particular double minimum structure in the simulated spectrum arises from the overlap of PERY based vibronic transitions. The fact that in the simulated CD spectrum the positive amplitude at 600 nm is larger than the negative amplitude at either 520 or 560 nm can be attributed to appreciable interchromophoric coupling between the PERY and OPV moieties.

We now turn to analysis of the absorption and CD spectra for complex **2**. We adopt a structural model for aggregates of this complex (Figure 9a) that is very similar to the one used before to model the properties for aggregates of complex **1**. The electronic coupling  $V$  between the distant OPV chromophores on opposite sides of the aggregate is calculated to be very small ( $V < 1$  meV). This gives collective excited states that are localized predominantly on the OPV chromophores and that are almost degenerate. In the calculation of the transition dipole moments for these quasidegenerate levels we have assumed that one level carries all the dipole strength, with the

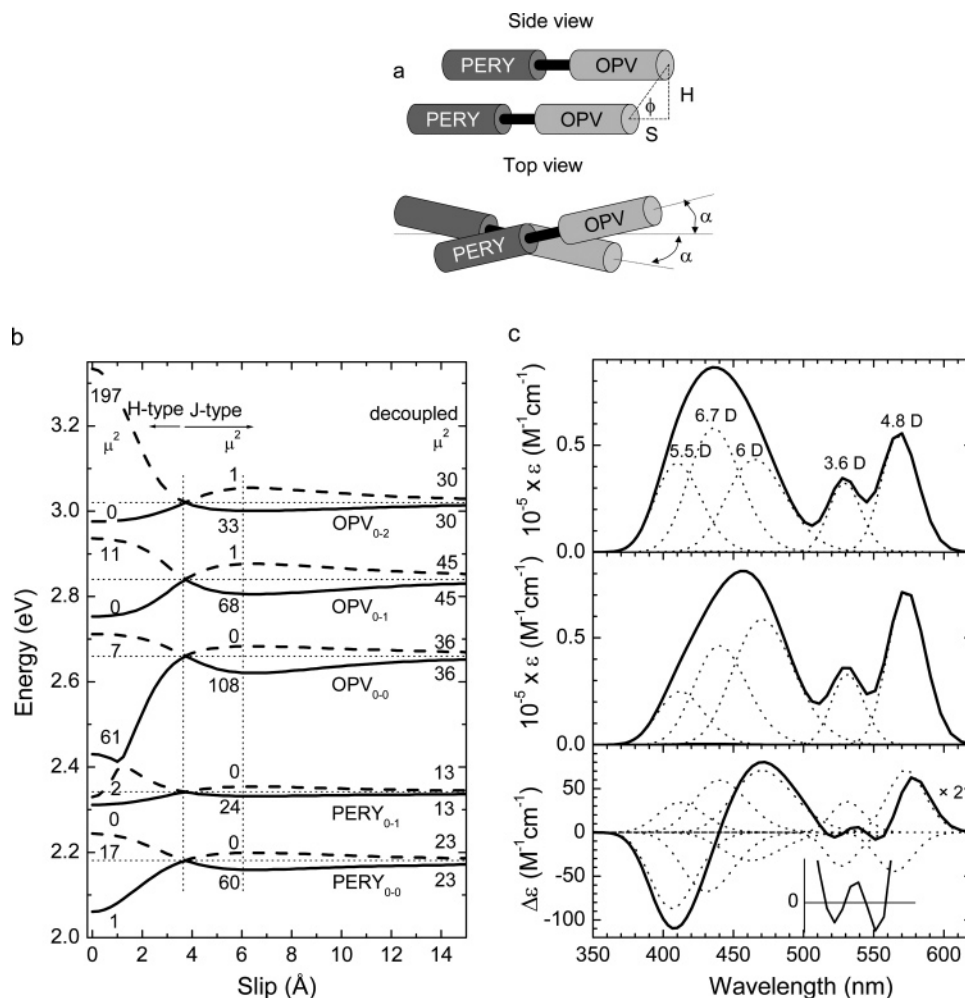


**Figure 8.** (a) Structure model for aggregates of complex **1**. (b and c) See caption Figure 7.

other level having a fully forbidden transition to the ground state. Also for this aggregate structure we find H- and J-type characteristics depending on  $S$ . The switching point between the two types of behavior is again around an  $S$  value of 3.5 Å (Figure 9b). For  $S = 9$  Å, the simulated absorption and CD spectra are shown. Comparing the low-temperature experimental CD spectra for aggregates of complex **1** and **2** we notice that the shape of the two spectra shows similarities but they have opposite sign. To match this change in sign we have reversed the twist angle  $\alpha$  of aggregate, which results in a sign reversal of the calculated CD effects. The slip  $S$  is taken to be the same for both aggregates and on the basis of their similar structure, the calculated CD spectra for aggregates of complex **1** and **2** shows strong similarities (Figure 9c).

Looking at the first vibronic absorption band of the PERY chromophore, we notice that the calculations predict a Davydov splitting of this band in a long wavelength component with negative CD and a component at shorter wavelength with positive CD. Here the CD effect is not *conservative*; the CD effect of the long wavelength transition has much larger amplitude than the band at shorter wavelength with a positive CD effect so that the areas under the positive and negative lobes of the bisignate Cotton effects are not equal. This result is also observed experimentally (Figure 4b). In the calculation, this nonconservation arises from mixing of the PERY and OPV based transitions and the calculated CD effects are conservative when integrating over both the OPV and PERY transitions.<sup>67</sup>

The structural model as shown in Figure 8a has also been used to simulate the absorption spectra for aggregates of

complex **3**. The results are shown in Figure 10. For this complex, the OPV and Cl-PERY based transitions overlap making analysis of the spectra more difficult. The simulated spectra are able to reproduce the red shift of the maximum of the absorption band (Figure 5) and also the bisignate Cotton effect can be accounted for.

In summary, the red shifted absorption bands observed for the aggregates can be rationalized in terms of aggregate structures in which the hydrogen-bonded complexes are stacked on top of each other with a considerable slip fraction. For complexes **1** and **3**, the packing of the dyads is expected to occur in a parallel rather than an antiparallel fashion. The types of packing proposed allow for orbital overlap between  $\pi$ -orbitals localized on OPV and PERY moieties that face each other in the aggregate. Thus the type of packing proposed allows for direct electronic interactions between donor and acceptor chromophores in the aggregate.

**Photoinduced Electron Transfer in the Aggregates.** We now turn to the photophysical properties of complexes **1–3** in the aggregated state. We studied the excited-state properties with fluorescence and subpicosecond pump–probe spectroscopy.

In contrast to the tetrachlorinated PBI-3 derivatives, phenoxy-substituted compounds PBI-1 and PBI-2 are strongly photoluminescent. Accordingly, a good indication for the presence of a photoinduced charge-transfer reaction can be obtained by monitoring the intensity of the PERY luminescence because this chromophore has the lowest excited-state energy. For complex **2**, the photoluminescence intensity of the PERY moiety at 590 nm was monitored as a function of temperature (Figure 11). At

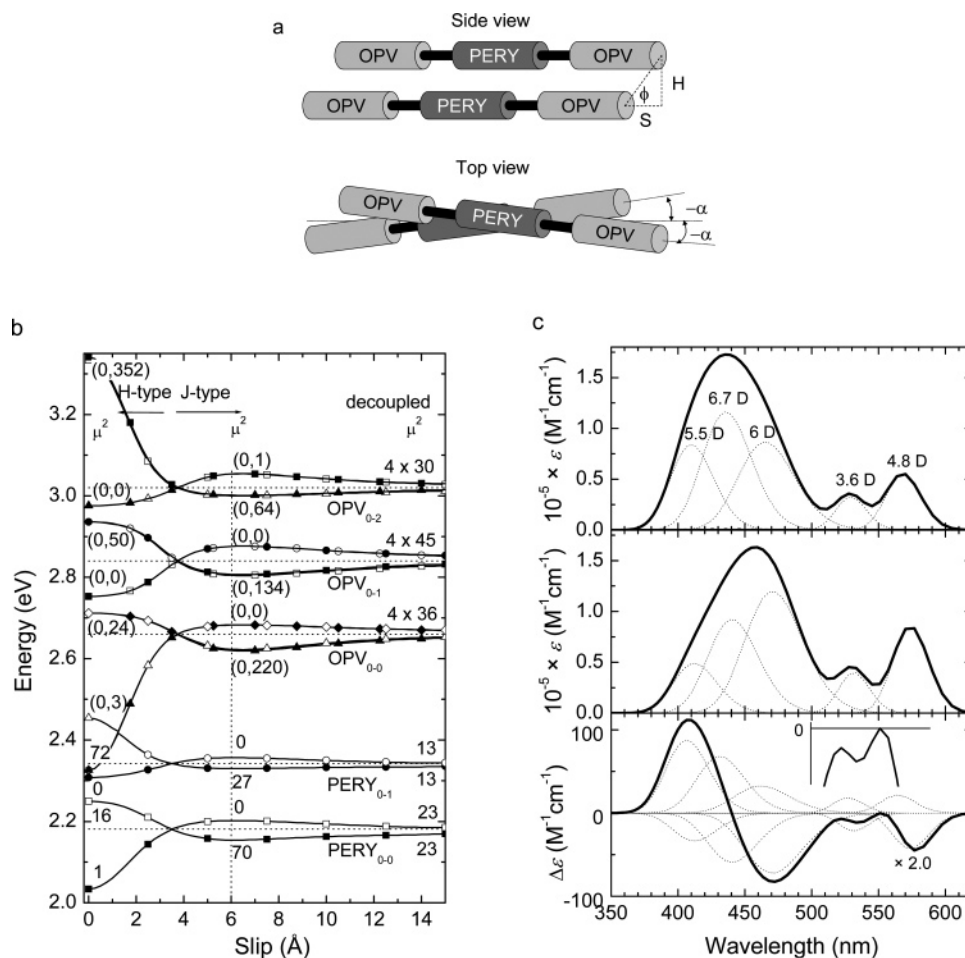


**Figure 9.** (a) Structure model for aggregates of complex 2. (b and c) See caption Figure 7 except for  $\alpha = -2.5^\circ$ .

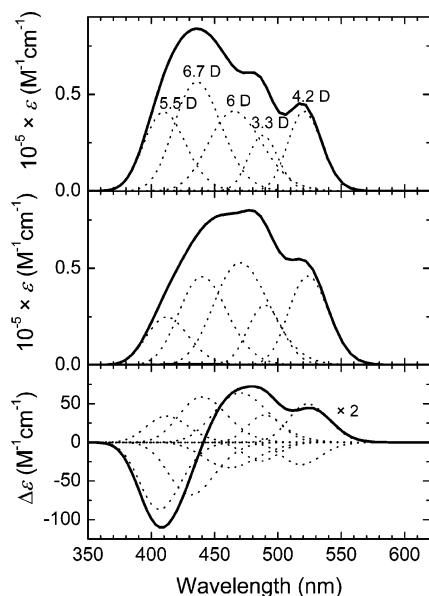


**Figure 10.** Simulated spectra for complex 3 using the structural model illustrated in Figure 8 ( $S = 9$  Å,  $H = 5$  Å,  $\alpha = 5^\circ$ ). Upper panel: absorption for uncoupled chromophores. Middle panel: absorption spectrum for the aggregate. Only one of the two vibronic Davydov levels carries appreciable intensity. Lower panel: simulated CD.

elevated temperatures, the luminescence intensity is considerably higher than that at room temperature, indicating luminescence quenching in aggregated species. The transition temperature of  $55^\circ\text{C}$  (at a concentration of  $5 \times 10^{-6}$  M) is similar to the

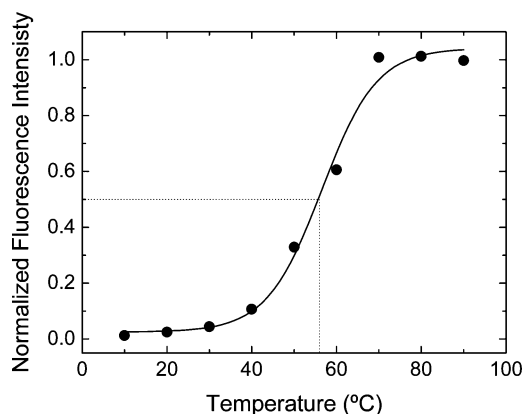


**Figure 11.** Normalized photoluminescence intensity at 590 nm for a  $5 \times 10^{-6}$  M solution of complex 2 in MCH recorded at different temperatures.

transition temperature observed in the absorption and CD experiments.<sup>43</sup> Aggregate formation itself can also lead to luminescence quenching, especially for H-type aggregates. However, J-type aggregation, as observed for complex 2, generally does not result in a large luminescence quenching because the lowest exciton state is radiatively coupled to the ground state. The almost quantitative quenching of the luminescence is therefore attributed to a photoinduced charge-transfer reaction in the supramolecular structure.

The driving force for photoinduced electron transfer ( $-\Delta G_{\text{CS}}$ ) can be predicted by using the Weller equation (eqs 4 and 5)<sup>68</sup> with experimentally determined values for the oxidation and reduction potentials of the donor and acceptor as well as the



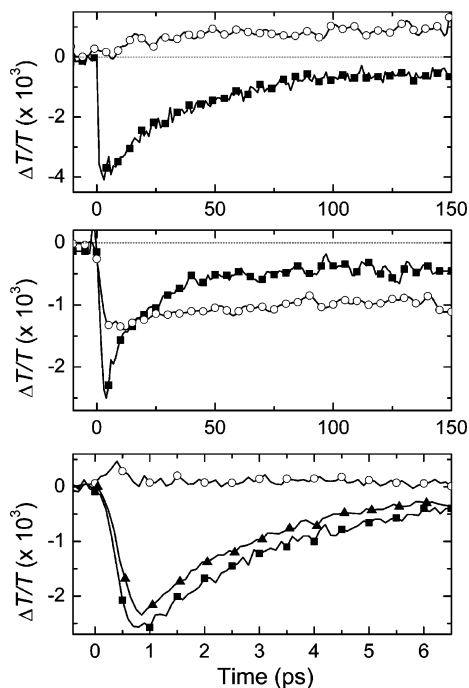


**Figure 12.** Transient photoinduced absorption traces in MCH for complex **1** (top,  $2 \times 10^{-4}$  M), complex **2** (middle,  $5 \times 10^{-5}$  M), and complex **3** (bottom,  $1 \times 10^{-4}$  M) at  $T = 20$  (solid squares), 50 (solid triangles), and 80 °C (open circles). The excitation wavelength is 455 nm and the PIA signal was detected at 1450 nm.

energy of the excited state from which the electron transfer proceeds. The latter set of values is listed in Table 1.

$$-\Delta G_{\text{CS}} = E(S_1) - G_{\text{CS}} \quad (4)$$

$$G_{\text{CS}} = e[E_{\text{ox}}(\text{D}) - E_{\text{red}}(\text{A})] - \frac{e^2}{4\pi\epsilon_0\epsilon_s R_{\text{cc}}} - \frac{e^2}{8\pi\epsilon_0} \left( \frac{1}{r^+} + \frac{1}{r^-} \right) \left( \frac{1}{\epsilon_{\text{ref}}} - \frac{1}{\epsilon_s} \right) \quad (5)$$

Actually, according to eqs 4 and 5, the charge separated state of complex **2** will be 0.51 eV above the PERY( $S_1$ ) level in MCH ( $\epsilon_s = 2.020$ ) at infinite distance between the donor and acceptor moieties ( $R_{\text{cc}} = \infty$ ). The energy of the charge separated state only drops below that of the PERY( $S_1$ ) state for  $R_{\text{cc}} < 13$  Å. This distance is shorter than the separation between the centers of the OPV and PERY moieties in the isolated (nonaggregated) hydrogen-bonded complex. The photoluminescence quenching (Figure 11) in the aggregated state, however, strongly suggests the occurrence of an electron-transfer reaction and therefore transient photoinduced absorption (PIA) spectroscopy was employed for complexes **1** and **2** (Figure 12). By taking into account the low driving force for a charge separation reaction, it is surprising to see that for both complexes **1** and **2** a clear PIA signal can be detected when the OPV radical cation band is monitored at 1450 nm (Figure 12). Moreover, the measured charge separation occurs within 1 ps ( $k_{\text{CS}} > 10^{12} \text{ s}^{-1}$ ) for both complexes. Hence, the electron transfer occurs within the time resolution of the used setup. Taking into consideration an aggregate structure as shown in Figure 9 the experimental evidence for electron transfer and the predictions of the Weller equations can be reconciled assuming that electron transfer does not proceed via the hydrogen bonds between OPV and PERY but occurs through the cofacial contacts between OPV-PERY units that arise when the hydrogen-bonded complexes pack on top of each other with a large slip  $S$ . In this way, the distance

**TABLE 2: Rate Constants for Charge Separation ( $k_{\text{CS}}$ ) and Charge Recombination ( $k_{\text{CR}}$ ) in MCH and Toluene at Room Temperature<sup>a</sup>**

compd	$k_{\text{CR}}(\text{MCH}) (\text{s}^{-1})$	$k_{\text{CS}}(\text{TOL}) (\text{s}^{-1})$	$k_{\text{CR}}(\text{TOL}) (\text{s}^{-1})$
complex <b>1</b>	$2.8 \times 10^{10}$		
complex <b>2</b>	$6.3 \times 10^{10}$		
complex <b>3</b>	$5 \times 10^{11}$		
Ph-OPO	$2 \times 10^9$	$3 \times 10^{11}$	$< 8 \times 10^8$
Cl-OPO	$8 \times 10^{10}$	$1.5 \times 10^{12}$	$1.6 \times 10^{10}$

<sup>a</sup> For all compounds  $k_{\text{CS}}(\text{MCH}) > 10^{12} \text{ s}^{-1}$ .

between the cation and anion formed after charge transfer is much smaller, resulting in a higher driving force making the electron transfer energetically allowed also in a highly apolar solvent. For complex **1**, the distances between OPV and PERY, the redox levels, and lowest excited-state energy are very similar to those of complex **2** and also in this case the rapid electron transfer can be rationalized by assuming that it occurs via cofacial OPV-PERY contacts.

The rates for electron transfer in the hydrogen-bonded complexes **1** and **2** can also be compared with the rates obtained for the covalently linked Ph-OPO compound. In the apolar solvent toluene no evidence for aggregate formation could be obtained for Ph-OPO and in this solvent, photoinduced charge separation proceeds rather slowly (Table 2) in comparison with the charge generation in the aggregates of **1** and **2**. This is consistent with the view that electron transfer proceeds via the cofacial OPV-PERY contacts.

Apart from the charge separation, the charge recombination can also be followed by using PIA in the picosecond time domain. We find that the rates for recombination in MCH [ $k_{\text{CR}}(\text{MCH})$ ] for aggregates of **1** and **2** are very similar in magnitude (Table 2), both being 2 orders of magnitude higher than those for the Ph-OPO model compound dissolved in toluene. This observation can be rationalized in terms of the electron transfer and recombination taking place in cofacial OPV-PERY pairs. Due to the close distance between the centers the energy of the charge-separated state (CSS) is lower in comparison with the CSS state in Ph-OPO when dissolved in toluene. As the charge recombination is in the inverted region the closer proximity of the donor and acceptor can explain a more rapid recombination. In addition the electronic coupling between donor and acceptor necessary for electron transfer may be larger for the cofacial OPV-PERY pair than for two chromophores in a linear array such as in Ph-OPO. The stronger coupling would also contribute to the higher recombination rates. Interestingly, the values for  $k_{\text{CR}}(\text{MCH})$  for the aggregates of **1** and **2** are considerably higher than those for aggregates of Ph-OPO in MCH (see also Figure S2).<sup>43,44</sup> Also for the aggregate of Ph-OPO in MCH the high rates for  $k_{\text{CR}}(\text{MCH})$  were rationalized in terms of electron transfer in cofacial pairs of donor and acceptor units. The absorption and circular dichroism spectra of the complexes **1** and **2** (Figure 3, Figure 4) together with Ph-OPO (see ref 44) indicate that all three systems are aggregated in a J-type fashion, but with a subtle difference in the packing geometry that could influence the kinetics.

The absorption and circular dichroism spectra (Figures 3 and 4) reveal that the aggregates dissolve when solutions of complexes **1** and **2** in MCH are heated. Consequently, one expects a loss of the OPV radical cation signal in the transient absorption at elevated temperatures. Indeed, for complex **1** the radical cation signal is not observed at 80 °C, but for complex **2** a clear signal with a rise time of less than 1 ps can be detected at 80 °C. The lifetime of the charge-separated state increases somewhat unexpectedly from 16 ps at 20 °C to more than 200

ps at 80 °C for complex **2**. The lower rate for charge recombination at higher temperatures may result from molecularly dissolved hydrogen-bonded complexes or small loosely bound aggregates present. The absorption and circular dichroism spectra show that indeed some aggregated species can be present at elevated temperatures because the maximum in the absorption spectrum is still shifting and a small circular dichroism signal can be detected (Figure 4). The distance between the redox centers in these complexes is larger than that in the  $\pi$ - $\pi$  stacked assembly with close contact between OPV and PERY of neighboring triads resulting in a decrease of the rate for charge recombination.

A key difference between the phenoxy and the chlorine substituted PERY moieties is the reduction potential, which have been determined at  $-1.17$  and  $-0.80$  V for PBI-1 and PBI-3, respectively (Table 1). In addition, there is a considerable difference in  $S_1$  energies of PBI-1 (2.12 eV) and PBI-3 (2.38 eV). The sum of the 0.37 and 0.26 eV differences in reduction potential and singlet energy results in a 0.63 eV larger driving force for charge separation ( $-\Delta G_{CS}$ ) at the same distance for complex **3** in comparison with complex **1** or **2**. The driving force, however, decreases significantly in less polar solvents (eqs 4 and 5).<sup>68</sup> In MCH, the transient PIA trace recorded at the low-energy absorption of the OPV radical cation<sup>39</sup> indicates that at room temperature OPV radical cations are created after photoexcitation (Figure 12). The rise of the signal occurs within 1 ps, indicating that the rate for charge separation ( $k_{CS}$ ) is faster than  $10^{12}$  s<sup>-1</sup>. The decay of the signal can be fitted with an exponential decay having a time constant of 2 ps, equivalent to a charge recombination rate ( $k_{CR}$ ) of  $5 \times 10^{11}$  s<sup>-1</sup>. The recombination in the aggregate is considerably faster than the recombination of photoinduced carriers in the model compound Cl-OPO in toluene (Table 2), which indicates electron transfer via cofacial interactions of donor and acceptor in the stack.

At an elevated temperature of 50 °C, a large fraction of complex **3** is still aggregated (Figure 5), which is confirmed by the kinetics of the transient absorption of the OPV radical cation (Figure 12) that is similar to the one at 20 °C. When the sample was heated to 90 °C, the circular dichroism almost disappeared and the absorption spectrum showed a considerable shift of the PERY maximum compared to the spectrum recorded at room temperature. This implies that the aggregates and the hydrogen bond between the OPV and PERY chromophores are broken at 90 °C.<sup>56</sup> In accordance, Figure 12 shows that no OPV radical cation signal can be detected on a picosecond time scale at 90 °C because the loss of connectivity between the OPV and PERY chromophores in the molecularly dissolved state inhibits electron transfer.

## Conclusions

A fast photoinduced charge-transfer reaction has been observed for aggregated OPV-PERY systems connected via a diaminotriazine-bisimide hydrogen bonding couple in MCH solutions. The reaction likely occurs intermolecularly between OPV and PERY chromophores of two different hydrogen-bonded OPV-PERY arrays that are packed in a slipped, J-type fashion, thereby creating short OPV-PERY distances between adjacent layers in the stack. The absorption and circular dichroism spectra were used to assess the molecular orientation of the chromophores of the aggregates with use of a coupled oscillator model. The experimental spectra which show red shifts of the absorption bands upon aggregation and accompanying Cotton effects can be rationalized assuming a packing with a considerable slip between adjacent hydrogen-bonded complexes.

This slip reduced the distance between donor and acceptor moieties, which may explain the fast charge recombination in terms of charge transfer between adjacent H-bonded complexes.

The results presented here imply that the charge transfer kinetics are largely determined by subtle differences in the supramolecular organization of the chromophores, especially for packing in a J-type fashion. A comparison of the molecularly dissolved and aggregated OPV-PERY systems leads to the conclusion that aggregation and the creation of short intermolecular distances are equally important parameters in photoinduced charge-transfer reactions as the redox potentials or excited-state energy.

## Experimental Section

**Materials.** The synthetic routes to OPV-Tr,<sup>43</sup> PBI-2,<sup>46</sup> Ph-OPO,<sup>43</sup> and Cl-OPO<sup>52</sup> have been reported before.

*N*-(3,4,5-Tridodecyloxyphenyl)-1,6,7,12-tetra(4-tert-butylphenoxy)perylene-3,4:9,10-tetracarboxylic acid bisimide (PBI-1). A mixture of 1,6,7,12-tetra(4-tert-butylphenoxy)perylene-3,4:9,10-tetracarboxylic acid bisanhydride (0.30 g, 0.30 mmol), 3,4,5-tris(*n*-dodecyl-1-yloxy)aniline (200 mg, 0.31 mmol), and Zn(OAc)<sub>2</sub> (47 mg, 0.21 mmol) in 15 mL of quinoline was stirred under Ar at 180 °C for 1.5 h. After cooling, the mixture was poured into 300 mL of 1 N HCl, and the precipitate was collected by filtration, washed with water and MeOH, and dried in a vacuum. The crude product was added to a mixture of ammonium acetate (5.0 g, 64.9 mmol) and 30 mL of propionic acid and refluxed for 15 h. Then 200 mL of water was added and the precipitate was isolated by filtration and dried in a vacuum and the crude product was further purified by silica gel column chromatography with CH<sub>2</sub>Cl<sub>2</sub> as eluent. After the solvent was evaporated, the product was redissolved in CH<sub>2</sub>Cl<sub>2</sub> (10 mL) and precipitated by adding MeOH (30 mL) and then isolated by filtration as dark-purple crystalline powder (78 mg, 16%). <sup>1</sup>H NMR (400 MHz, CDCl<sub>3</sub>, 25 °C, TMS):  $\delta$  8.42 (s, 1H, N-H), 8.24 (s, 2H, H<sub>perylene</sub>), 8.20 (s, 2H, H<sub>perylene</sub>), 7.23 (m, 8H, Ar-H), 6.86 (d,  $J$  = 8.8 Hz, 4H, Ar-H), 6.81 (d,  $J$  = 8.8 Hz, 4H, Ar-H), 6.39 (s, 2H, Ar-H), 3.97 (t, 2H,  $J$  = 6.4 Hz, 2H, OCH<sub>2</sub>), 3.88 (t, 4H,  $J$  = 6.2 Hz, OCH<sub>2</sub>), 1.7–1.8 (m, 6H), 1.5–1.1 (m, 90 H), 0.86 (m, 9H, CH<sub>3</sub>). MS (MALDI-TOF) calculated for C<sub>106</sub>H<sub>134</sub>N<sub>2</sub>O<sub>11</sub> 1611.0 *m/z*, found 1611.6 [M]<sup>+</sup>. Elemental analysis (%) calculated for C<sub>106</sub>H<sub>134</sub>N<sub>2</sub>O<sub>11</sub>: C 78.97, H 8.38, N 1.74. Found: C 78.93, H 8.37, N 1.66. UV/vis (CH<sub>2</sub>-Cl<sub>2</sub>):  $\lambda_{max}/nm$  ( $\epsilon/M^{-1} cm^{-1}$ ) 583 (47000), 543 (28800), 454 (17600), 269 (48000).

*N*-(3,4,5-Tridodecyloxyphenyl)-1,6,7,12-tetrachloroperylene-3,4:9,10-tetracarboxylic acid bisimide (PBI-3). A mixture of 1,6,7,12-tetrachloroperylene-3,4:9,10-tetracarboxylic acid bisanhydride (800 mg, 1.51 mmol), 3,4,5-tridodecyloxyaniline, (200 mg, 0.31 mmol), and Zn(OAc)<sub>2</sub> (90 mg, 0.41 mmol) in 30 mL of quinoline was stirred under Ar for 180 °C at 1.5 h. After cooling to room temperature, the mixture was poured into 400 mL of 1 N HCl, and the precipitate was separated by filtration, washed with water and MeOH, and dried in a vacuum. Then the resulting crude product was added to a mixture of ammonium acetate (5.0 g, 64.9 mmol) and 30 mL of propionic acid and refluxed for 15 h. Then 200 mL water was added and the precipitate was separated by filtration, dried in a vacuum, and purified by silica gel column chromatography with CH<sub>2</sub>-Cl<sub>2</sub>/EtOAc (95:5) as eluent. After the solvent was evaporated, the product was redissolved in CH<sub>2</sub>Cl<sub>2</sub> (10 mL) and precipitated by adding MeOH (30 mL) and then isolated by filtration as orange powder (210 mg, 61%). <sup>1</sup>H NMR (400 MHz, CDCl<sub>3</sub>, 25 °C, TMS):  $\delta$  8.77 (s, 1H, N-H), 8.72 (s, 2H, H<sub>perylene</sub>), 8.69

(s, 2H,  $H_{\text{peryl}}$ ), 6.48 (s, 2H, Ar–H), 4.03 (t, 2H,  $J = 6.6$  Hz, 2H, OCH<sub>2</sub>), 3.95 (t, 4H,  $J = 6.4$  Hz, OCH<sub>2</sub>), 1.7–1.9 (m, 6H), 1.5–1.1 (m, 54H), 0.87 (m, 9H, CH<sub>3</sub>). MS (MALDI-TOF): calculated for C<sub>66</sub>H<sub>82</sub>N<sub>2</sub>O<sub>7</sub>Cl<sub>4</sub> 1154.5  $m/z$ ; found 1154.8 [M]<sup>+</sup>. Elemental analysis (%) calculated for C<sub>66</sub>H<sub>82</sub>N<sub>2</sub>O<sub>7</sub>Cl<sub>4</sub>: C 68.50, H 7.14, N 2.42. Found: C 68.48, H 7.17, N 2.40. UV/vis (CH<sub>2</sub>–Cl<sub>2</sub>):  $\lambda_{\text{max}}$ /nm ( $\epsilon/\text{M}^{-1} \text{ cm}^{-1}$ ) 522 (40200), 489 (28300), 427 (11100), 275 (32300).

**Methods.** UV/vis absorption spectra were recorded on a Perkin-Elmer Lambda 900 spectrophotometer and circular dichroism measurements were performed on a Jasco J-600 spectropolarimeter. Fluorescence spectra were recorded on an Edinburgh Instruments FS920 double-monochromator spectrometer with a Peltier-cooled red-sensitive photomultiplier. The femtosecond laser system used for pump–probe experiments has been described earlier.<sup>44,52</sup>

Cyclic voltammograms were measured in 0.1 M tetrabutylammonium hexafluorophosphate (TBAPF<sub>6</sub>) as a supporting electrolyte in dichloromethane with a Potentiostat Wenking POS73 potentiostat. The working electrode was a Pt disk (0.2 cm<sup>2</sup>), the counter electrode was a Pt plate (0.5 cm<sup>2</sup>), and a saturated calomel electrode (SCE) was used as reference electrode, calibrated against Fc/Fc<sup>+</sup>.

A description of the used coupled oscillator model for the calculations of the excited-state energy levels and circular dichroism spectra can be found in the Supporting Information.

**Acknowledgment.** This work has been supported by CW-NWO in the PIONIER program, the DFG (grant Wu 317/5), and the European Integrated project NAIMO (NMP4-CT-2004-500355). The research of Stefan Meskers has been made possible by a fellowship of the Royal Dutch Academy of Arts and Sciences.

**Supporting Information Available:** A detailed description of the used parameters to model the absorption and circular dichroism spectra. This material is available free of charge via the Internet at <http://pubs.acs.org>.

## References and Notes

- Huber, R. *Angew. Chem., Int. Ed.* **1989**, 28, 848–869.
- Moser, C. C.; Keske, J. M.; Warncke, K.; Farid, R. S.; Dutton, P. L. *Nature* **1992**, 355, 796–802.
- The Photosynthetic Reaction Center*, Deisenhofer, J.; Norris, J. R., Eds.; Academic Press: New York, 1993.
- Blankenship, R. E. *Molecular Mechanisms of Photosynthesis*; Blackwell Science: Oxford, U.K., 2002.
- Wasielewski, M. R. *Chem. Rev.* **1992**, 92, 435–61.
- Gust, D.; Moore, T. A.; Moore, A. L. *Acc. Chem. Res.* **1993**, 26, 198–205.
- Gust, D.; Moore, T. A.; Moore, A. L. *Acc. Chem. Res.* **2001**, 34, 40–48.
- Paddon-Row, M. N. *Acc. Chem. Res.* **1994**, 27, 18–25.
- Guldi, D. M. *Chem. Soc. Rev.* **2002**, 31, 22–36.
- Moore, T. A.; Moore, A. L.; Gust, D. *Philos. Trans. R. Soc. London B* **2002**, 357, 1481–1498.
- Imahori, H.; Mori, Y.; Matano, Y. *J. Photochem. Photobiol. C* **2003**, 4, 51–83.
- Imahori, H. *Org. Biomol. Chem.* **2004**, 2, 1425–1433.
- Tecilla, P.; Dixon, R. P.; Slobodkin, G.; Alavi, D. S.; Waldeck, D. H.; Hamilton, A. D. *J. Am. Chem. Soc.* **1990**, 112, 9408–9410.
- Balzani, V.; Scandola, F. *Supramolecular Photochemistry*; Ellis Horwood: Chichester, UK, 1991.
- Harriman, A.; Magda, D. J.; Sessler, J. L. *J. Phys. Chem.* **1991**, 95, 1530–1532.
- Harriman, A.; Kubo, Y.; Sessler, J. L. *J. Am. Chem. Soc.* **1992**, 114, 388–390.
- Turro, C.; Chang, C. K.; Leroi, G. E.; Cukier, R. I.; Nocera, D. G. *J. Am. Chem. Soc.* **1992**, 114, 4013–4015.
- Sessler, J. L.; Wang, B.; Harriman, A. *J. Am. Chem. Soc.* **1993**, 115, 10418–10419.
- Sessler, J. L.; Wang, B.; Harriman, A. *J. Am. Chem. Soc.* **1995**, 117, 704–714.
- De Rege, P. J. F.; Williams, S. A.; Therien, M. J. *Science* **1995**, 269, 1409–1413.
- Roberts, J. A.; Kirby, J. P.; Nocera, D. G. *J. Am. Chem. Soc.* **1995**, 117, 8051–8052.
- Sessler, J. L.; Wang, B.; Springs, S. L.; Brown, C. T. In *Comprehensive Supramolecular Chemistry*; Atwood, J. L., Davies, J. E. D., MacNicol, D. D., Vögtle, F., Murakami, Y., Eds.; Pergamon: Oxford, UK, 1996; Vol. 4, pp 311–336.
- Kirby, J. P.; Roberts, J. A.; Nocera, D. G. *J. Am. Chem. Soc.* **1997**, 119, 9230–9236.
- Ward, M. D. *Chem. Soc. Rev.* **1997**, 26, 365–376.
- Piotrowski, P. *Chem. Soc. Rev.* **1999**, 28, 143–150.
- Prasad, E.; Gopidas, K. R. *J. Am. Chem. Soc.* **2000**, 122, 3191–3196.
- Chang, C. J.; Brown, J. D.; Chang, M. C. Y.; Baker, E. A.; Nocera, D. G. In *Electron Transfer in Chemistry*; Balzani, V., Ed.; Wiley-VCH, Weinheim, Germany, 2001; Vol. 3, pp 409–461.
- Myles, A. J.; Branda, N. R. *J. Am. Chem. Soc.* **2001**, 123, 177–178.
- Smitha, M. A.; Prasad, E.; Gopidas, K. R. *J. Am. Chem. Soc.* **2001**, 123, 1159–1165.
- Smitha, M. A.; Gopidas, K. R. *Chem. Phys. Lett.* **2001**, 350, 86–92.
- Sessler, J. L.; Sathiosatham, M.; Brown, C. T.; Rhodes, T. A.; Wiederrecht, G. *J. Am. Chem. Soc.* **2001**, 123, 3655–3660.
- Schenning, A. P. H. J.; van Herrikhuyzen, J.; Jonkheijm, P.; Chen, Z.; Würthner, F.; Meijer, E. W. *J. Am. Chem. Soc.* **2002**, 124, 10252–10253.
- Segura, M.; Sánchez, L.; De Mendoza, J.; Martín, N.; Guldi, D. M. *J. Am. Chem. Soc.* **2003**, 125, 15093–15100.
- Hoeben, F. J. M.; Jonkheijm, P.; Meijer, E. W.; Schenning, A. P. H. J. *Chem. Rev.* **2005**, 105, 1491–1546.
- Sánchez, L.; Martín, N.; Guldi, D. M. *Angew. Chem., Int. Ed.* **2005**, 44, 5374–5382.
- Sessler, J. L.; Jayawickramarajah, J.; Gouloumis, A.; Torres, T.; Guldi, D. M.; Maldonado, S.; Stevenson, K. J. *Chem. Commun.* **2005**, 1892–1894.
- Imahori, H. *J. Phys. Chem. B* **2004**, 108, 6130–6143.
- Van der Boom, T.; Hayes, R. T.; Zhao, Y.; Bushard, P. J.; Weiss, E. A.; Wasielewski, M. R. *J. Am. Chem. Soc.* **2002**, 124, 9582–9590.
- Van Hal, P. A.; Meskers, S. C. J.; Janssen, R. A. J. *Appl. Phys. A* **2004**, 79, 41–46.
- Fujitsuka, M.; Masuhara, A.; Kasai, H.; Oikawa, H.; Nakanishi, H.; Ito, O.; Yamashiro, T.; Aso, Y.; Otsubo, T. *J. Phys. Chem. B* **2001**, 105, 9930–9934.
- Fuller, M. J.; Sinks, L. E.; Rybtchinski, B.; Giaimo, J. M.; Li, X.; Wasielewski, M. R. *J. Phys. Chem. A* **2005**, 109, 970–975.
- Rybtchinski, B.; Sinks, L. E.; Wasielewski, M. R. *J. Am. Chem. Soc.* **2004**, 126, 12268–12269.
- Würthner, F.; Chen, Z.; Hoeben, F. J. M.; Osswald, P.; You, C.-C.; Jonkheijm, P.; van Herrikhuyzen, J.; Schenning, A. P. H. J.; van der Schoot, P. P. A. M.; Meijer, E. W.; Beckers, E. H. A.; Meskers, S. C. J.; Janssen, R. A. J. *J. Am. Chem. Soc.* **2004**, 126, 10611–10618.
- Beckers, E. H. A.; Meskers, S. C. J.; Schenning, A. P. H. J.; Chen, Z.; Würthner, F.; Marsal, P.; Beljonne, D.; Cornil, J.; Janssen, R. A. J. *J. Am. Chem. Soc.* **2006**, 128, 649–657.
- Sinks, L. E.; Rybtchinski, B.; Iimura, M.; Jones, B. A.; Goshe, A. J.; Zuo, X.; Tiede, D. M.; Li, X.; Wasielewski, M. R. *Chem. Mater.* **2005**, 17, 6295–6303.
- Würthner, F.; Thalacker, C.; Sautter, A.; Schärfl, W.; Ibach, W.; Hollricher, O. *Chem. Eur. J.* **2000**, 6, 3871–3886.
- Ilhan, F.; Gray, M.; Rotello, V. M. *Macromolecules* **2001**, 34, 2597–2601.
- Kawasaki, T.; Tokuhira, M.; Kimizuka, N.; Kunitake, T. *J. Am. Chem. Soc.* **2001**, 123, 6792–6800.
- Thalacker, C.; Würthner, F. *Adv. Funct. Mater.* **2002**, 12, 209–218.
- Schenning, A. P. H. J.; Jonkheijm, P.; Peeters, E.; Meijer, E. W. *J. Am. Chem. Soc.* **2001**, 123, 409–416.
- Chen, Z.; Debije, M. G.; Debaerdemaeker, T.; Osswald, P.; Würthner, F. *ChemPhysChem* **2004**, 5, 137–140.
- Beckers, E. H. A.; Meskers, S. C. J.; Schenning, A. P. H. J.; Chen, Z.; Würthner, F.; Janssen, R. A. J. *J. Phys. Chem. A* **2004**, 108, 6933–6937.
- Prokhorenko, V. I.; Steengaards, D. B.; Holzwarth, A. R. *Biophys. J.* **2003**, 85, 3173–3186.
- Didraga, C.; Klugkist, J. A.; Knoester, J. A. *J. Phys. Chem. B* **2002**, 106, 11474–11486.
- Spano, F. C.; Zhao, Z.; Meskers, S. C. J. *J. Chem. Phys.* **2004**, 120, 10594–10604.

- (56) Würthner, F. *Chem. Commun.* **2004**, 1564–1579.
- (57) Harada, N.; Nakanishi, K. *Circular Dichroic Spectroscopy. Exciton Coupling in Organic Stereochemistry*; Oxford University Press: Oxford, UK, 1983.
- (58) Gierschner, J.; Mack, H.-G.; Lüer, L.; Oelkrug, D. *J. Chem. Phys.* **2002**, *116*, 8596.
- (59) Narwark, O.; Meskers, S. C. J.; Peetz, R.; Thorn-Csanyi, E.; Bäessler, H. *Chem. Phys.* **2003**, *294*, 1–15.
- (60) Peeters, E.; Marcos, A.; Meskers, S. C. J.; Janssen, R. A. J. *J. Chem. Phys.* **2000**, *112*, 9445–9454.
- (61) Michl, J.; Thulstrup, E. W. *Spectroscopy with Polarized Light*; VHC Publications Inc.: New York, 1986.
- (62) Witkowski A.; Moffitt, W. *J. Chem. Phys.* **1960**, *33*, 872–875.
- (63) Fulton, R. L.; Gouterman, M. *J. Chem. Phys.* **1961**, *35*, 1059–1071.
- (64) Sterzel, M.; Pilch, M.; Pawlikowski, M. T.; Gawronski, J. *J. Chem. Phys.* **2003**, *291*, 251–260.
- (65) Neuteboom, E. E.; Meskers, S. C. J.; Van Hal, P. A.; Van Duren, J. K. J.; Meijer, E. W.; Janssen, R. A. J.; Dupin, H.; Pourtois, G.; Cornil, J.; Lazzaroni, R.; Brédas, J.-L.; Beljonne, D. *J. Am. Chem. Soc.* **2003**, *125*, 8625–8638.
- (66) Kasha, M. *Radiat. Res.* **1963**, *20*, 55–70.
- (67) In a previous publication we argued that the nonconservation may also originate from a shift in the conformational P  $\rightleftharpoons$  M equilibrium of the twisted perylene moiety.<sup>43</sup> At the moment we cannot completely exclude a contribution to the CD effect of the helical twist of the PERY chromophore, yet the model calculations presented here, which do not take into account such conformational equilibrium, provide a possible explanation of the observed nonconservation in the CD spectrum of the PERY based transition.
- (68) Weller, A. Z. *Phys. Chem.* **1982**, *133*, 93–98.